ELSEVIER

Journal of Photochemistry and Photobiology A: Chemistry 95 (1996) 143–155

Journal of PHOTOCHEMISTRY AND PHOTOBIOLOGY A:CHEMISTRY

Fluorescence loss mechanism due to large-amplitude motions in derivatives of 2,2′-bipyridyl exhibiting excited-state intramolecular proton transfer and perspectives of luminescence solar concentrators

Friedrich Vollmer, Wolfgang Rettig *,[1]

Iwan N.-Stranski-Institut, Technische Universität Berlin, Straße des 17. Juni 112, D-10623 Berlin, Germany

Received 29 August 1995; accepted 13 October 1995

Abstract

Fluorescence quantum yields and lifetimes as functions of temperature and solvent polarity are compared for two different hydroxy derivatives of 2,2′-bipyridyl. Both dyes show strongly red-shifted excited-state intramolecular proton transfer (ESIPT) fluorescence at all temperatures investigated. In protic solvents, the ESIPT emission is of a more allowed nature and somewhat blue shifted, owing to specific solvatation. A strong difference in behaviour can, however, be observed for the non-radiative losses. The symmetric dye **1** possesses large fluorescence quantum yields, whereas sizeable fluorescence quantum yields from **2** could only be obtained under high viscosity conditions. Increased solvent polarity leads to enhanced fluorescence losses. These facts and the comparison with quantum chemical calculations for planar and twisted structures of **1** and **2** are interpreted as evidence for a photochemically reached low-lying state with charge separation (twisted intramolecular charge transfer (TICT)), responsible for these fluorescence losses and especially active for **2**. For **1** in aprotic solvents, this reaction is discussed within the quantum-chemical extension of electron transfer theory and shown to involve nuclear tunnelling. In addition to this viscosity-dependent decay channel, **2** also decays via a viscosity-independent (presumably n–π^*) channel. The identification of the TICT and n–π^* non-radiative channels allows a new approach to the development of highly fluorescent ESIPT dyes with very large Stokes shift for use in fluorescence solar collectors or other devices utilizing the principle of fluorescence-based light-pipes.

Keywords: Fluorescence; Proton transfer; Electron transfer; TICT; Solar concentrators

1. Introduction

Fluorescence solar collectors or luminescent solar concentrators (LSCs) [1–7] can in principle constitute a very cost-effective way of transforming solar energy directly into electricity. Instead of using a large surface of photovoltaic cells, the collection area is covered with one or more layers of glass plates containing a fluorescent dye. As shown in Fig. 1, light absorbed by such a dye and re-emitted as fluorescence is channelled towards the side surfaces through multiple total internal reflections where it can become highly concentrated depending on the ratio of collection area to that of the side surfaces. The advantages of such arrangements are (i) use of considerably less photovoltaic material, (ii) light concentration also under conditions of diffuse illumination (cloudy sky) and (iii) less heating of the photovoltaic material.

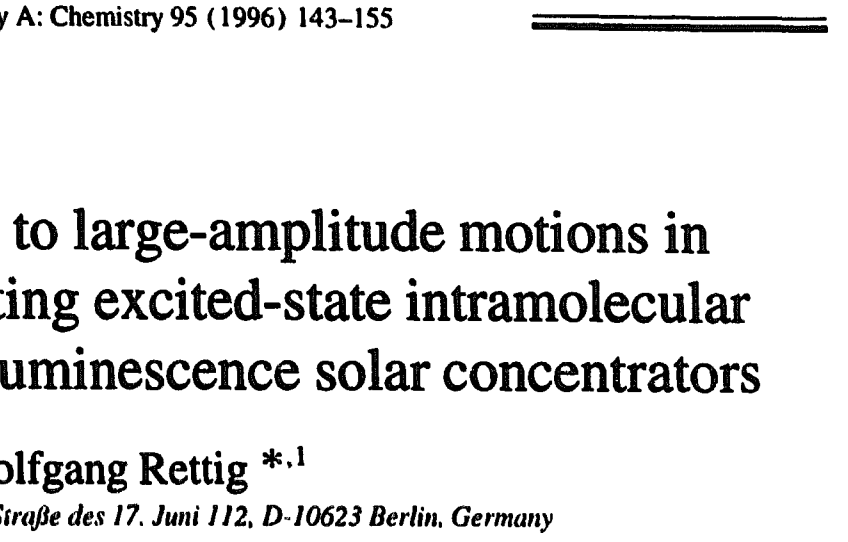

Fig. 1. Schematic representation of a fluorescent solar concentrator. It works in both sunny and cloudy conditions via absorption of the incident photons by a fluorescent dye embedded in the plate and multiple total internal reflection of the re-emitted and red-shifted light towards the edges which are covered with a photovoltaic material. Photons emitted inside the 'cone of loss' leave the plate because they do not meet the condition for total internal reflection. If a dye centre absorbs a photon which has already been emitted from another dye centre (reabsorption), the same intrinsic losses (cone of loss and nonradiative decay processes) occur again.

* Corresponding author.

[1] Present address: Institut für Physikalische und Theoretische Chemie, Humboldt-Universität zu Berlin, Bunsenstraße 1, D-10117 Berlin, Germany.

SSDI 1010-6030(95)04252-0

Widespread use of LSCs, however, is still hampered by some inherent shortcomings of present-day LSCs, and thus the development of possible ways to overcome them is highly promising. In recent years, the following weak points of LSCs have been successfully tackled.

(i) The partial coverage of the solar spectrum by the absorption spectrum of the dye can be enhanced by energy transfer or by using multiple layers of LSCs covering different spectral ranges.

(ii) The long-term photostability of the dyes is one of the most serious problems especially if organic dyes are used instead of inorganic absorbing materials (which present other disadvantages such as low absorption coefficients and very narrow bands [6]). However, at least one class of dyes has been found (perylimides) where long-term photostability is sufficient [7], even for the much more stringent conditions present in a tunable solid state dye laser [8]. Moreover, the use of inorganic glass material for embedding organic dyes (sol–gel glass technique [9,10]) can enhance the dye stability [2].

(iii) For large concentration ratios, the problem of reabsorption of the emitted fluorescence photons by the dye becomes increasingly important, especially for cases where absorption and fluorescence spectra overlap significantly. Every reabsorption process leads to intrinsic losses due to incomplete total internal reflection (trapping efficiency $\phi_{tr} \approx 75\%$ for poly(methyl methacrylate) (PMMA) [3]) and to non-radiative relaxation ($\phi_{nr} = 1 - \phi_f$ where ϕ_f is the fluorescence quantum yield). For example, even for ideal fluorescence dyes ($\phi_f = 1$), ten reabsorption processes lower the collection efficiency $\phi_{col} = (\phi_{tr}\phi_f)^n$ (where n is the number of reabsorption processes) by a factor of $1/(0.75)^{10} = 18$ and this factor increases to 18 000 (corresponding to 99.99% loss of light-trapping efficiency) for medium efficient dyes ($\phi_f = 0.50$). A simple way of eliminating this important loss factor consists in decoupling absorption and emission spectra, and thus eliminating the reabsorption possibility for example by way of an adiabatic photochemical reaction. Excited-state intramolecular proton transfer (ESIPT) dyes prove to be especially promising in this respect because they show extremely large Stokes shifts and negligible spectral overlap of absorption and emission in solution and also in PMMA glasses usable as collector plates (see below). Several highly fluorescent ESIPT dyes are known, some of which, e.g. 2-phenyl-3-hydroxy-flavone [12–17] and 3,3′-dihydroxy-2,2′-bipyridyl (**1**) [18–23] have been used as laser dyes [12,22,24,25]. Another possible approach for spectral decoupling is to use the red-shifted emission from twisted intramolecular charge transfer (TICT) states [26–29] some of which show high fluorescence efficiencies [30–32].

In the following, we concentrate on ESIPT dyes and try to elucidate possible sources of intramolecular fluorescence quenching. Unfortunately, the vast majority of known ESIPT dyes show high ϕ_{nr} (low ϕ_f) in fluid solution. This emphasizes the importance of controlling these non-radiative channels for the development of new ESIPT dyes for LSCs. As an example, we study the closely related dyes **1** and **2**:

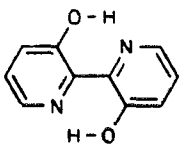

1

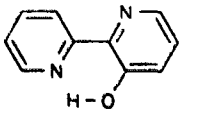

2

They differ in the fluorescence efficiency by about three orders of magnitude at room temperature [20]. Using the solvent viscosity, solvent polarity and temperature dependence of the non-radiative rate constant k_{nr} and comparing it with quantum-chemical calculations, we can identify a charge transfer state connected with a large-amplitude motion (TICT state) being responsible for the major part of k_{nr} in this type of flexible molecule.

2. Experimental details

Compounds **1** and **2** were a gift from Professor Anna Grabowska and Dr. Hanna Bulska (Warsaw) and were used as received. The spectral properties of **1** corresponded to those reported in the literature [20], whereas for **2** some deviations of the spectra (see Fig. 2) from those reported in the literature [20] were found. Solvents (mostly Merck Uvasol) were of Spectrograde purity. Absorption spectra were measured on a Cary 17 spectrometer. Corrected fluorescence spectra were measured on a Perkin–Elmer 650/60 spectrofluorimeter, and fluorescence quantum yields were determined relative to quinine sulphate in 0.1 N H_2SO_4 ($\phi_f = 0.55$ [33]) and are corrected for changes in solvent refractive index and solute absorption with temperature. Low temperature fluorescence lifetimes were measured with the single-photon-counting technique using synchrotron radiation from BESSY (single-bunch mode) as excitation source. The equipment used has been described elsewhere [34]. The instrument response function had a half width of 550 ps, and the iterative reconvolution procedure allowed us to determine lifetimes down to approximately 0.1 ns. Fluorescence decays for **1** were monoexponential at all temperatures ($\chi^2 \leq 1.2$).

Quantum-chemical calculations were performed using the CNDO/S formalism [35,36] by taking into account all singly excited configurations below 15 eV in the configuration interaction (CI) procedure. ([36] was used with the original parameters in an updated version able to cope with 139 atomic orbitals.) Idealized geometry was assumed if not otherwise stated, with $r_{CC} = 1.4$ Å, $r_{CH} = 1.08$ Å, $r_{OH} = 0.97$ Å, $r_{CN} = 1.40$ Å, $r_{CO} = 1.42$ Å and angles C–C–C of 120°, and C–O–H 109°.

[2] Proton transfer dyes can also be highly photostable in organic polymers as shown by their application in polyethylene greenhouse covers [11].

3. Experimental and theoretical results

3.1. Steady-state and time-resolved spectroscopy

Fluorescence and absorption spectra of **1** and **2** in solvents of different polarity are displayed in Fig. 2. Both compounds show the characteristically red-shifted ESIPT fluorescence. Even for **1** in PMMA glass, the spectral separation is complete. There is little solvent effect on the fluorescence spectra which are virtually identical for **1** in all aprotic solvents studied ($\lambda_{max} = 500$ nm), and somewhat blue-shifted in alcohols ($\lambda_{max} = 480$ nm) but independent of the type of alcohol used. Table 1 shows that the fluorescence quantum yields drastically differ for the two compounds investigated. However, even for the highly fluorescent compound **1**, the ϕ_f values in aprotic polar solvents and in homologous *n*-alcohols clearly show a tendency for decreasing ϕ_f with increasing solvent polarity. No such correlation is found with solvent viscosity, at least for the aprotic solvents used (Table 1). As shown below for **2**, viscosity effects become operative only at much lower temperatures, where the viscosities are several orders of magnitude higher.

Fig. 3 displays the temperature dependence of fluorescence quantum yield ϕ_f and fluorescence lifetime τ_f for **1** in different solvents. For decreasing temperature, ϕ_f and τ_f increase in parallel to each other, consistent with a temperature-independent fluorescence rate constant $k_f \approx 12 \times 10^7\ s^{-1}$ for **1** in ethanol. At 77 K, the τ_f values in all solvents investigated converge to a common lifetime τ_f (77 K) = 4.8 ± 0.2 ns. This behaviour clearly shows the presence of a temperature-dependent intramolecular fluorescence quenching process. Fig. 3(b) shows the corresponding temperature-dependent non-radiative decay rate constants k_{nr}^T calculated from the following equation and plotted vs. $1/T$:

$$k_{nr}^T = \tau_f^{-1}(T) - \tau_f^{-1}(77\ K) \quad (1)$$

This plot shows that, at low temperatures, k_{nr}^T is much slower in ethanol than in the other solvents used, and the temperature dependence (activation energy) is greater in alcohol than in aprotic solvents. The derived Arrhenius parameters are collected in Table 2. This table also contains the measured lifetimes at 77 K and the comparison of experimental k_f and k_{nr} values. Aprotic polar solvents of different polarities show similar k_f values ($8 \times 10^7\ s^{-1}$) whereas the k_f values for alcohols are significantly increased ($12 \times 10^7\ s^{-1}$). This lends support to the idea that the fluorescent species for **1** in aprotic and protic solvents differ.

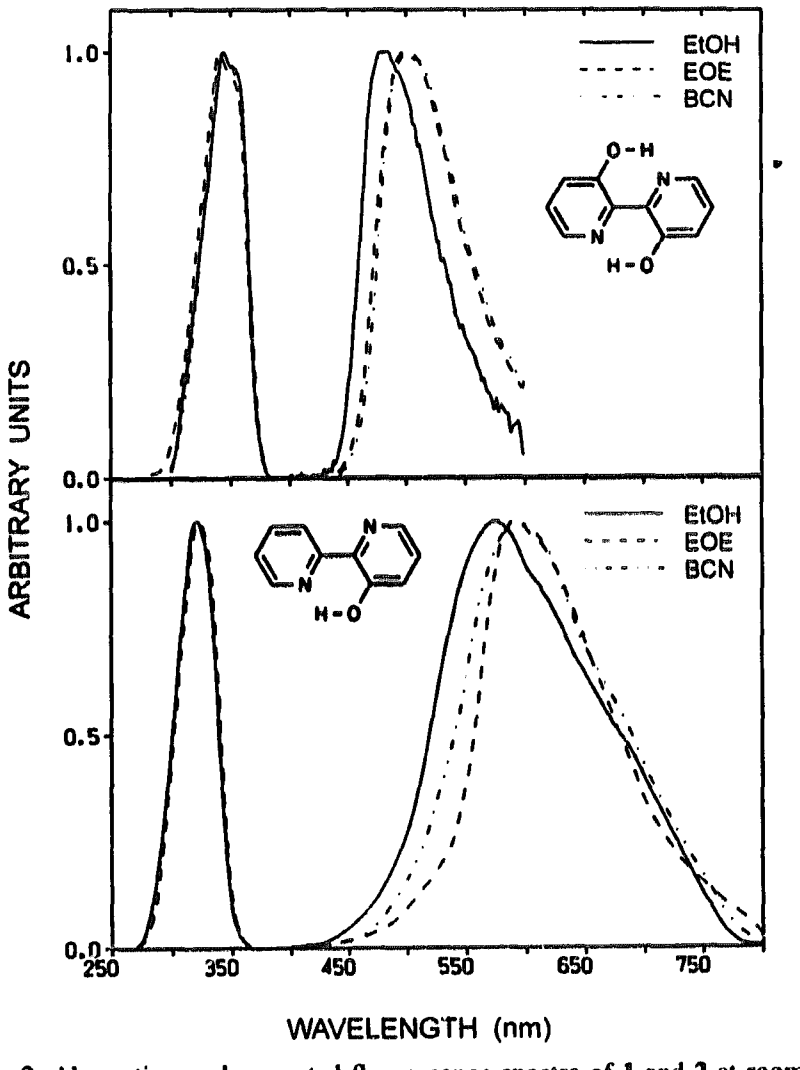

Fig. 2. Absorption and corrected fluorescence spectra of **1** and **2** at room temperature in different solvents.

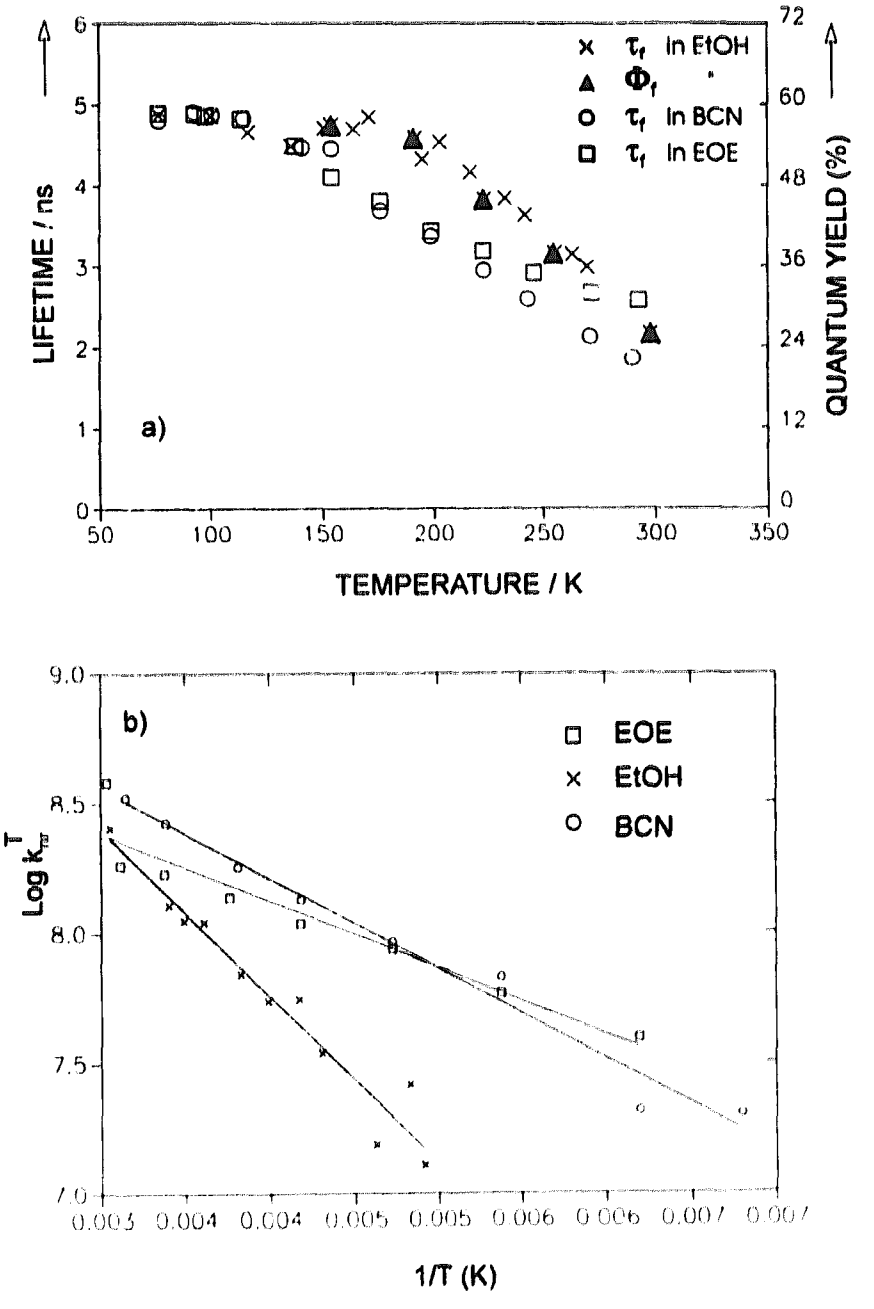

Fig. 3. (a) Fluorescence decay times of **1** as a function of temperature in different solvents, and comparison with the temperature dependence of the fluorescence quantum yield. (b) The derived temperature dependent non-radiative decay constants k_{nr}^T in an Arrhenius plot.

Table 1
Fluorescence quantum yields of 1 and 2 in aprotic solvents of different polarity and the protic *n*-alcohol series, in aerated solutions at room temperature, where the solvent polarities are expressed on the Δf scale; the measured extinction coefficient for the long-wavelength absorption maximum is also given

Solvent	Δf [a]	η [b] (cP)	$\phi_f(1)$	$\phi_f(2)$	$\epsilon(1)$ ($l\,mol^{-1}\,cm^{-1}$)	$\epsilon(2)$ ($l\,mol^{-1}\,cm^{-1}$)
Aprotic solvents						
2-Methylbutane	0	0.22	0.32	–	17500	14900
3-Methylpentane	0	0.32	0.32 [c]	0.001 [d]		
Cyclohexane	0	0.66	0.31 [d]	–		
Diethyl ether	0.167	0.22	0.21	–		
Tetrahydrofurane	0.21	0.46	0.21	–		
n-Butyronitrile	0.275	0.60	0.15	–		
Protic solvents						
n-Butanol	0.263	2.95	0.36 [d]	–		
n-Propanol	0.273	2.25	0.31	–		
Ethanol	0.289	1.20	0.28	0.00015		
Methanol	0.308	0.55	0.25	–		

[a] $\Delta f = (\epsilon - 1)/(2\epsilon + 1) - (n^2 - 1)(2n^2 + 1)$ with ϵ the dielectric constant and n the refractive index.
[b] From [37].
[c] From [20].
[d] From [23].

Table 2
Arrhenius parameters for temperature-dependent fluorescence quenching (k_{nr}^T) of 1 in different solvents, and comparison of lifetimes at 77 K and at room temperature, and of the derived k_f and k_{nr} values

Solvent	E_A [a] (kJ mol^{-1})	log A [b]	τ_f (77 K) ($\times 10^{-9}$ s)	τ_f (298 K) ($\times 10^{-9}$ s)	k_f (298 K) [c] ($\times 10^7 s^{-1}$)	k_{nr}^T (298 K) [d] ($\times 10^7 s^{-1}$)	k_{nr}^{tot} (298 K) [e] ($\times 10^7 s^{-1}$)
Aprotic solvents							
2-Methylbutane	3.3 (±0.3)	8.4 (±0.2)	4.63	3.51	8.55	6.8	19.9
Diethyl ether	4.9 (±0.3)	9.2 (±0.1)	4.89	2.58	8.14	18.31	30.6
n-Butyronitrile	7.2 (±0.5)	9.8 (±0.1)	4.80	1.86	8.06	32.93	45.7
Protic solvents							
Butanol	15.3 (±2.5)	10.7 (±0.5)	4.77	2.92	12.3	13.3	21.9
Propanol	14.6 (±0.3)	10.7 (±0.1)	4.77	2.72	11.4	15.8	25.4
Ethanol	14.2 (±1.3)	10.9 (±0.3)	4.87	2.24	12.5	24.1	32.1
Methanol	11.3 (±0.5)	10.6 (±0.1)	4.96	1.26	19.8	59.2	59.5

[a] Activation energy.
[b] A is the pre-exponential factor.
[c] $k_f = \phi_f/\tau_f$.
[d] From Eq. (1).
[e] $k_{nr}^{tot} = (1 - \phi_f)/\tau_f$.

3.2. Multiple-relaxations scheme in aprotic and protic solvents

A closer look at the temperature dependence of τ_f in alcohols supports this conclusion. Fig. 4 displays $\tau_f(T)$ for 1 in a series of alcohols. It can be seen that, at low temperatures, there is a temperature range of little change in τ. This range extends to higher temperatures for longer-chain alcohols.

We interpret this behaviour as being due to the more complicated photophysical behaviour of 1 in alcohols compared with aprotic solvents. Scheme 1 contrasts the two models which we propose. The wavy arrows indicate temperature-independent non-radiative processes.

In aprotic solvents (Scheme 1(a)), two subsequent relaxation processes are possible, leading first quantitatively (in picoseconds) to the intramolecular proton transfer product P* and then, much more slowly (in about 3 ns in butyronitrile), towards a charge transfer (CT) state A* with non-emissive properties mainly responsible for the solvent-polarity- and temperature-dependent non-radiative losses. The CT nature of A* can be concluded from the observation that the temperature-dependent non-radiative decay process k_{nr}^T increases for more polar solvents (Tables 1 and 2). This is consistent with an assumed symmetry-breaking process between the ESIPT product P* (double-proton transfer [18,24], symmetric electronic structure, essentially zero

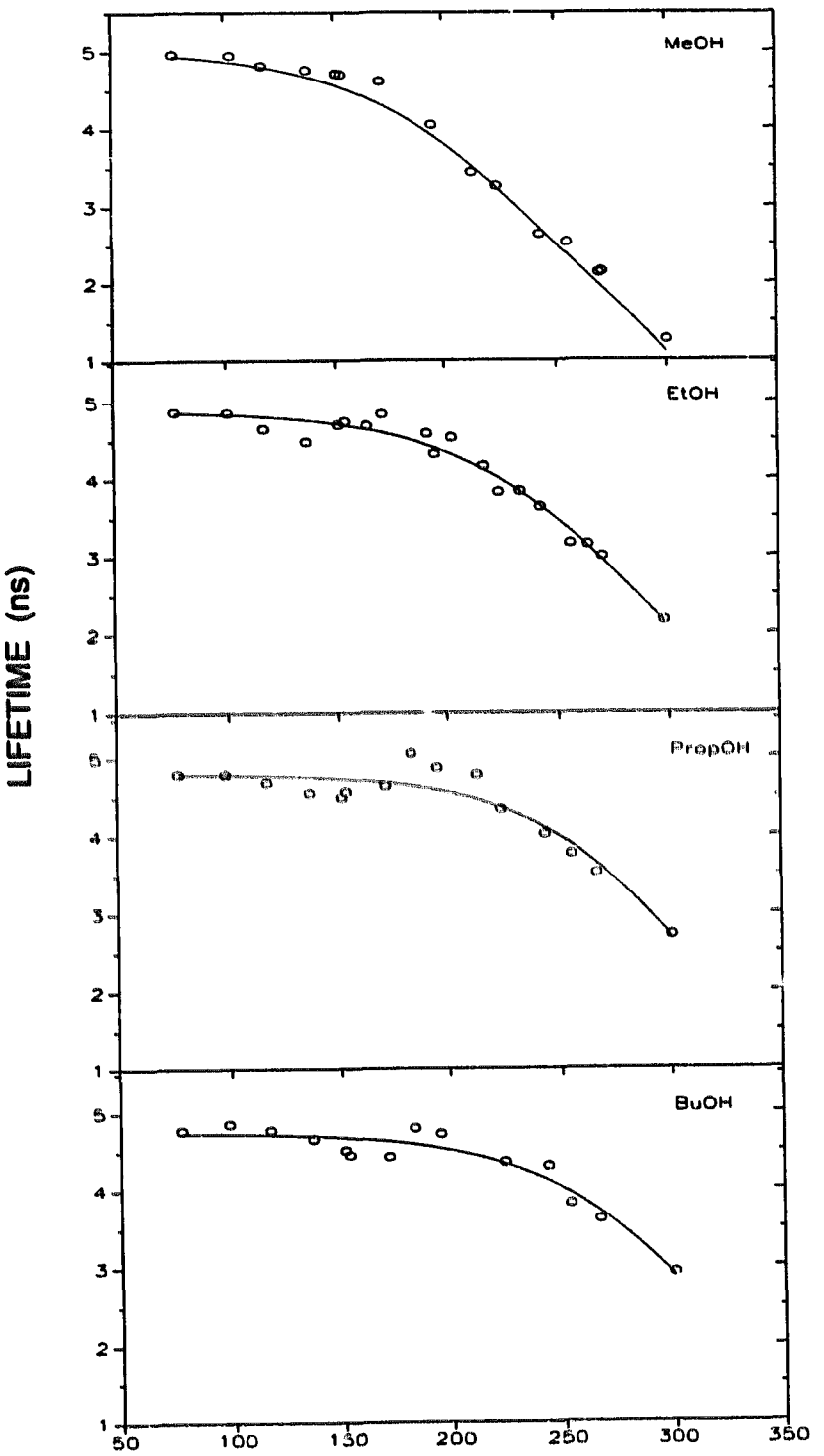

Fig. 4. Fluorescence decay times of 1 as a function of temperature in different *n*-alcanols.

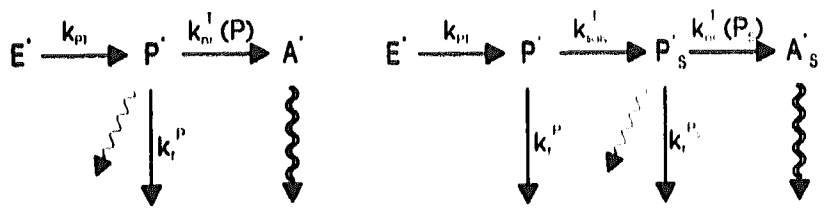

Scheme 1. ESIPT, solvation and deactivation process for 1: (a) aprotic solvents; (b) protic solvents.

dipole moment [21,24,38,39]) and the quenching state A* (charge transfer; large dipole moment). More polar solvents preferentially stabilize A* and accelerate the quenching reactions leading from P* to A* (see, however, below for the possibility of nuclear tunnelling in aprotic solvents).

As judged from the larger size of the total non-radiative decay rate constant k_{nr}^{tot} compared with k_{nr}^{T} (Table 2), P* has still another temperature- and polarity-independent non-radiative decay channel leading towards the ground state (around $1 \times 10^8\ s^{-1}$ for nearly all solvents). Oxygen quenching ($k_q[O_2] < 0.2 \times 10^8\ s^{-1}$ at room temperature for the solvents used) cannot be its source because it is temperature dependent. We therefore propose that it could be due to an involvement of the n–π^* state or to an intersystem crossing process. A further possible explanation involves reduction in $\phi_f(P^*)$ due to incomplete population of P* (through non-radiative losses in E*), but this is less likely because of the high value of the k_{PT} rate constant and the absence of E* fluorescence.

In protic solvents (Scheme 1(b)), the intramolecular ESIPT product P* can relax within a short time towards a solvated state P_s^*, the possible nature of which could be an ESIPT state with additional single or double intermolecular hydrogen bond bridges to the alcoholic solvent. The ESIPT nature of P_s^* can be concluded from the fluorescence spectrum with large Stokes shift, but the different k_f value and the slight blue shift with respect to aprotic polar solvents prove this state to be somewhat different from the ESIPT state reached in the absence of a protic solvent surrounding (Fig. 2).

The solvated state P_s^* possesses a more allowed nature than P* (increased k_f, Table 2). From the blue-shifted emission, we can conclude that the solvent stabilization for the corresponding ground state is more important than for P*. As the intramolecular fluorescence quenching originates from the solvated state P_s^*, we assume that the product is also solvated (A_s^* in Scheme 1(b)). P_s^* possesses a higher activation energy for A_s^* formation than P* (from comparison of E_A in protic and aprotic solvents in Table 2). In the sequence of excited-state processes (Scheme 1(b)), A_s^* formation is therefore stopped first upon sufficient cooling (see the plateau regions in Fig. 4) and then the solvation process k_{solv}^{T} is slowed down such that the unsolvated intramolecular ESIPT product P* starts to emit significantly.

The transformation of P* into P_s^* can be followed using the fluorescence spectra; Fig. 5 shows the temperature dependence of the fluorescence spectra of 1 in protic ethanol and aprotic diethyl ether. Upon lowering the temperature, a slight blue shift is observed in ether, together with some structuring (intrinsic behaviour of P*). In ethanol, however, a red shift is observed for 1 upon lowering the temperature converging to a spectrum similar to that in diethyl ether (transformation of blue-shifted P_s^* into P*).

3.3. Comparison of bifunctional and monofunctional excited-state intramolecular proton transfer compounds

Fig. 6 displays the fluorescence lifetime behaviour of 2 in different solvents compared with that of 1. At all temperatures, biexponential decay kinetics are observed for 2. The short decay component is always of dominating importance

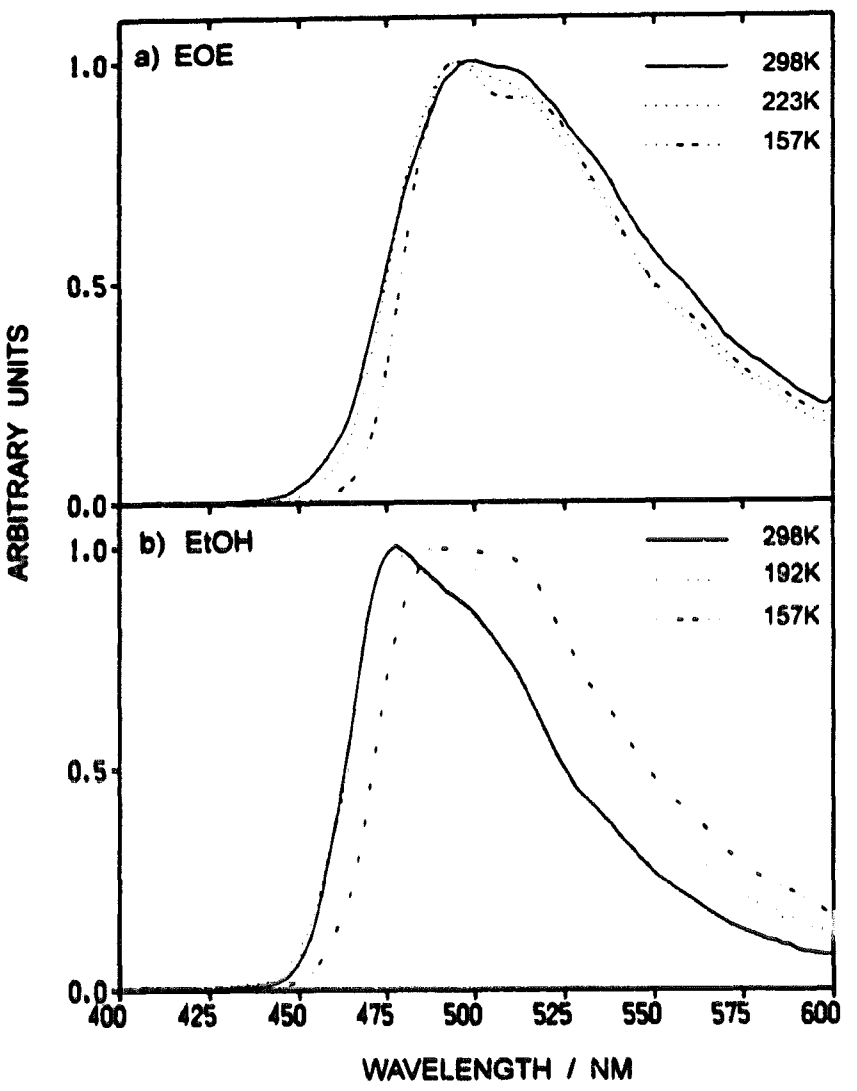

Fig. 5. Temperature dependence of the fluorescence spectra of 1 in (a) diethyl ether and (b) ethanol.

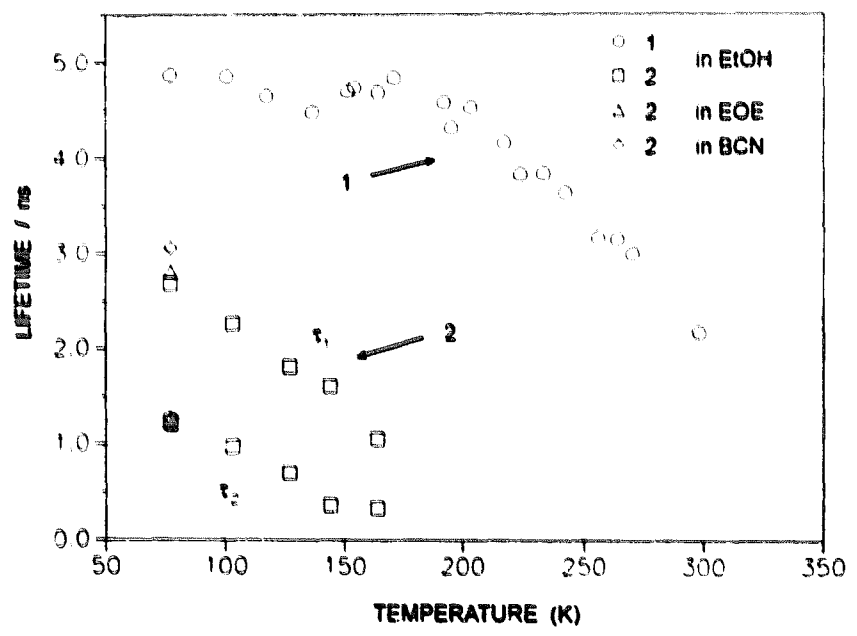

Fig. 6. Fluorescence decay components τ_1 and τ_2 of 2 in ethanol at low temperatures (Δ) as opposed to τ_f measured for 1 (○), and 77 K values for 2 in other solvents.

($A_1 > 70\%$) and shorter than our detection limit (about 100 ps) for temperatures above the freezing point of the solvents. Below it, the lifetimes lengthen (Fig. 6) and converge to a solvent independent value of about 1.3 ns for τ_1 and about 3 ns for τ_2. From the lifetime lengthening of τ_1 and τ_2 occurring significantly only below the freezing point of ethanol (156 K), we conclude that the main non-radiative decay is induced by a barrierless large-amplitude motion, probably twisting around the 2,2'-axis, which can be stopped by raising the solvent viscosity sufficiently far.

Fig. 6 also demonstrates clearly that the intramolecular fluorescence quenching behaviour of 1 and 2 differs strongly, that of 2 being faster by a large factor.

A direct comparison of the k_{nr}^T values for 1 and 2 is not possible with our data because the lifetime lengthening for 2 occurs at very low temperatures only where k_{nr}^T is already negligible for 1 (Fig. 6). We can, however, give a rough estimate for $k_{nr}^T(2)/k_{nr}^T(1) \gtrsim 200$ based on the Arrhenius extrapolation of the k_{nr} processes to 180 K.

Owing to this much faster photoreaction rate constant k_{nr}^T for 2, solvation of P* (rate constant k_{solv}^T) and photoreaction ($k_{nr}^T(P)$) in the unsolvated product P* can be expected to compete, and we have to use the more general kinetic Scheme 2 for the protic solvents.

Thus the possibility for simultaneous fluorescence from both unsolvated (P*) and solvated ESIPT species P_s is predicted and is supported by our observation of biexponential decay behaviour with both decay components being viscosity dependent (Fig. 6).

The decay parameters measured for 2 in ethanol somewhat depend on the emission wavelength. In the short-wavelength tail of the emission (500 nm) the relative weight of τ_1 is reduced (Table 3). We therefore conclude that two emissive species are observed: one with a red-shifted spectrum and shorter lifetime ($\tau_1 = 1.3$ ns at 77 K), and the other more centred towards the blue and with a longer intrinsic lifetime (about 3 ns at 77 K). We tentatively assign the blue-emitting longer-lifetime species to solvent-complexed P_s*, and the red-shifted short-lifetime species (τ_1) to uncomplexed P*.

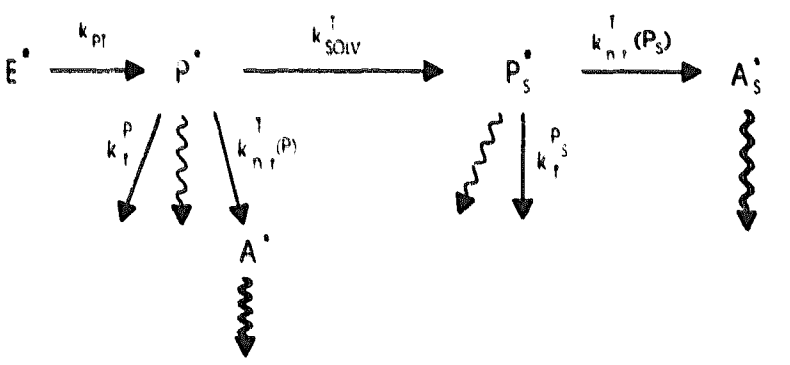

Scheme 2. Mechanistic scheme for 2 in protic solvents at low temperatures.

Table 3
Biexponential fit parameters (decay times τ_i) of the fluorescence decay of 2 in ethanol at low temperatures; the lifetimes are derived from globally fitting the decay curves at two emission wavelengths (500 and 580 nm; excitation at 320 nm); for a good fit of the decay curves, a third component was necessary which was either negligible in weight or below our time resolution

Temperature (K)	τ_1 (ns)	τ_2 (ns)	A_1/A_2 [a]	χ^2
164	0.35	1.02	5.50	1.18
127	0.54	1.20	2.10	1.20
77	1.32	3.00	4.00	1.16

[a] Ratio of pre-exponential factors at 580 nm; the weight of τ_2 increases at 500 nm.

3.4. Quantum-chemical calculations

The similar behaviours of **1** and **2** with respect to the ESIPT efficiency (absence of the short-wavelength band), and the strongly differing behaviours regarding the temperature-dependent non-radiative decay rate k_{nr}^{T} can be understood by considering the energetics of possible adiabatic photoproducts. We used quantum-chemical calculations for this purpose and compared the energies (relative to the ground state) of E*, P* and a presumed twisted A* species.

Table 4 contains a summary of the calculated energies of the lowest excited states of **1** and **2** in both E* and P* forms and the comparison of experimental with calculated fluorescence rate constants. For this purpose, the calculated oscillator strengths for the enol precursor E* (Scheme 1), $f = 0.295$ for **1**, and $f = 0.267$ for **2**, were compared with the experimental value ($f = 0.306$) for **1** determined from integrated absorption of **1** in 2-methylbutane ($\epsilon = 17\,500\,l\,mol^{-1}\,cm^{-1}$) as follows [40]:

$$f^{exp} = 4.32 \times 10^{-9} \int \epsilon \, d\tilde{\nu} \qquad (2)$$

The emissive processes from P* were similarly treated by comparing the experimental k_f values from the following equation with the calculated values:

$$k_f^{exp} = \frac{\phi_f}{\tau_f} \qquad (3a)$$

For this purpose, the following equation [40,41] was used to calculate approximate fluorescence rate constants k_f (in reciprocal seconds) from calculated f values and transition wavenumbers $\tilde{\nu}$ (in reciprocal centimetres) for P*:

$$k_f^{calc} = 0.661 \tilde{\nu}^2 f^{calc} \qquad (3b)$$

Table 4 leads to several important conclusions.

(i) Experimental and calculated k_f values for **1** ($(0.8–0.9) \times 10^8\ s^{-1}$) agree satisfactorily, consistent with emission from a P* state of π–π^* nature. The total decay rate τ_f^{-1} at 77 K ($2.0 \times 10^8\ s^{-1}$), which corresponds to the sum of radiative and non-radiative rate at this temperature, is about twice the value of that predicted on the basis of k_f alone.

(ii) For **2**, the k_f value calculated for P* ($0.8 \times 10^8\ s^{-1}$) and τ_f^{-1} at 77 K ($8.3 \times 10^8\ s^{-1}$) differ strongly. This indicates that even at 77 K a major non-radiative decay path is still present for **2**. This decay path could be due to efficient intersystem crossing or to coupling to a weakly or non-emitting ^1n–π^* state.

Tables 5 and 6 contain similar results derived for different geometric assumptions regarding P*. In the calculations for

Table 4
Calculated excited-state energies (CNDO/S) for **1** and **2** in the enol (E*) and the ESIPT form (P*), with standard geometries used as defined in the experimental section, together with the assignments, oscillator strengths f and calculated and experimental k_f values (see text)

State	Energy (eV)	f	Assignment	f^{exp} [a]	k_f^{calc} [b] ($\times 10^8\ s^{-1}$)	k_f^{exp} [c] ($\times 10^8\ s^{-1}$)	k_f^{abs} [d] ($\times 10^8\ s^{-1}$)
Compound 1, form E*							
S_1	3.22	0	n–π^*	0.306	1.65	–	1.72
S_2	3.57	0	n–π^*				
S_3	3.60	0.295	π–π^*				
S_4	4.34	0	π–π^*				
S_5	4.88	0.09	π–π^*				
Compound 1, form P*							
S_1	2.18	0	n–π^*	–	0.83	0.91	–
S_2	2.42	0.329	π–π^*				
S_3	2.83	0	n–π^*				
S_4	3.65	0	π–π^*				
S_5	3.67	0	n–π^*				
Compound 2, form E*							
S_1	3.06	0	n–π^*	0.273	1.72	–	1.73
S_2	3.59	0	n–π^*				
S_3	3.87	0.267	π–π^*				
S_4	4.36	0.003	π–π^*				
S_5	4.83	0.148	π–π^*				
Compound 2, form P*							
S_1	2.52	0	n–π^*	-	0.83	–	–
S_2	2.75	0.257	π–π^*				
S_3	3.76	0.05	π–π^*				
S_4	4.02	0	n–π^*				
S_5	4.40	0	n–π^*				

[a] From Eq. (2) and the ϵ value in Table 1.
[b] From Eq. (3b).
[c] From Eq. (3a).
[d] From integrated absorption using f^{exp} and $\tilde{\nu}_{exp}^2$ in Eq. (3b).

Table 5
Comparison of calculations for the ESIPT species P* of 1 using different geometries, as shown by the energies of the lowest π–π^* and n–π^* states (with respect to the ground state): variation in the C=O bond length R_{CO} (for R_{CC} = 1.4 Å)

R_{CO} (Å)	Energy (eV)	
	π–π^*	n–π^*
1.42	2.38	2.28
1.35	2.25	2.28
1.20	2.07	2.18

Table 6
Comparison of calculations for the ESIPT species P* of 1 using different geometries, as shown by the energies of the lowest π–π^* and n–π^* states (with respect to the ground state): variation in R_{CC}, the bond connecting the two rings (for R_{CO} = 1.2 Å)

R_{CC} (Å)	Energy (eV)	
	π–π^*	n–π^*
1.4	2.07	2.18
1.35	2.06	2.03
1.3	2.05	1.86

Table 7
Excited-state energies of 90° twisted ESIPT species of 1 and 2 with oscillator strength f and assignment; for comparison, results for the twisted enol form E* are also given

State	Energy (eV)	f	Assignment
Compound 1, form E*			
S_1	4.30	0	n–π^*
S_2	4.30	0	n–π^*
S_3	4.41	0.10	π–π^*
S_4	4.58	0.03	π–π^*
S_5	5.41	0	TICT
Compound 1, form P*			
S_1	2.63	0.0004	TICT
S_2	2.66	0.0005	TICT
S_3	2.78	0.26	π–π^*
Compound 2, form E*			
S_1	4.43	0.11	π–π^*
S_2	4.67	0.0013	n–π^*
S_3	4.70	0.028	π–π^*
S_4	4.72	0.017	TICT
Compound 2, form P*			
S_1	1.47	0.00001	TICT
S_2	2.85	0.0018	n–π^*
S_3	2.91	0.00005	TICT
S_4	3.64	0.003	n–π^*
S_5	3.72	0.14	π–π^*

Table 4, it was assumed that the positions of the heavy nuclei are the same for E* and P*, and only the enolic proton moves. The ESIPT form P*, however, is expected to possess some double-bond character in the bonds labelled R_{CC} and R_{CO} in Tables 5 and 6, which should lead to a shortening of these bonds in the excited-state equilibrium geometry. The results indicate that shortening of the C=O bonds may be an important geometrical relaxation. It leads to satisfactory agreement between the calculated energy (2.07 eV) and experimental energy (2.48 eV in aprotic solvents (Fig. 2)) of P* and to a reversal of π–π^* and n–π^* such that π–π^* becomes lower than n–π^*. This can explain the high fluorescence efficiency for 1; quenching by n–π^* states is negligible, and photochemical quenching by the A* state is also slow (see below).

The theoretical results indicate on the other hand that shortening of R_{CC} would lead to a preferential lowering of n–π^* and therefore fluorescence quenching and this relaxation coordinate is therefore thought, by comparison with the large quantum yields observed, to be of minor importance.

4. Discussion

4.1. A possible mechanism for photochemical intramolecular fluorescence quenching

From the above data on k_{nr}^T, it can be concluded that the temperature- and viscosity-dependent part k_{nr}^T is more than a hundredfold larger for 2 than for 1. We tried to correlate this difference with the energetics of a possible non-radiative adiabatic photoproduct A*.[3] As a most probable large-amplitude motion, the twisting around the 2,2′ double bond in the ESIPT product P* was considered. 90° twisting of this bond leads to orbital decoupling and thus to the possibility of low-lying TICT states [26–29,42]. Recent developments of the theory of TICT states [43–46] contain the description of both twisted single and twisted double bonds [28–31,42,46] by biradicaloid states.

Table 7 contains results of calculations for the lowest excited singlet states for the twisted geometry of the ESIPT product P* and also the twisted enol species E*, together with assignments. For both 1 and 2, the lowest excited state of the twisted P* species is of TICT nature and is therefore a candidate for the non-emissive quenching state A*. For P*(2), the TICT state calculated is of very low energy (1.47 eV), much lower than that of the locally excited (LE) π–π^* state of the twisted P* species (S_5, 3.72 eV) or of the "delocalized excited" (DE) state of the planar species (π–π^* state (2.75 eV) of P* in Table 4). For 1, on the contrary, the TICT energy (2.63 eV) is slightly higher than that of the π–π^* state of the untwisted P* (2.42 eV). We therefore propose that the strongly enhanced non-radiative decay rate k_{nr}^T as observed for 2 is due to an adiabatic photoreaction leading from P* towards a TICT state A* with low k_f and high intrinsic k_{nr} (non-radiative photochemical funnel [46]).

In spite of the much smaller non-radiative deactivation rates for 1, as displayed in Tables 1 and 2, their solvent polarity dependence can also be interpreted by the involve-

[3] A weak emission from A* cannot be excluded for 1. It would be very difficult to detect in the presence of the strongly emitting P* state.

ment of a TICT state A* as source of the increased non-radiative losses observed in more polar solvents. The calculations suggest that TICT formation may be endothermic for **1** or at least proceed over an activation barrier. As the structure of the TICT state is highly polar, this state should be preferentially stabilized in polar solvents with respect to the non-polar states of **1** (E* and P*). We therefore expect, according to the Bell–Evans–Polanyi principle [47], that the non-radiative decay rate should increase with increasing solvent polarity. In fact, the experimental ϕ_f data at room temperature (Table 1) and more precisely the temperature-dependent fluorescence loss rates k_{nr}^T (Table 2) clearly show an increased importance of k_{nr}^T (factor of about 5 for solvents used in Table 2) with increasing solvent polarity.

Table 7 also shows that a similar reaction process is unfavourable from the E* state; the TICT state of the twisted E species has a very high energy.

The calculations do not reproduce the charge separation for the twisted-geometry (TICT state) of **1** if a symmetric structure is used, but a slight asymmetry (lengthening and shortening of the C–C bonds by (±0.01 Å) leads to full charge separation (high dipole moment) connected with localization of frontier orbitals HOMO and LUMO on separate rings as observed similarly for calculations on twisted stilbene [48,49]. The symmetry-breaking process P* → A* in **1** induced by the polar solvent is therefore thought to be similar to the symmetry breaking in symmetric TICT-forming compounds such as 9,9′-bianthryl [29,50,51].

4.2. Nuclear tunnelling

As outlined above, the temperature-dependent non-radiative decay rate k_{nr}^T, as measured at room temperature, strongly depends on solvent polarity (Table 2), increasing in aprotic solvents from 7×10^7 s^{-1} (alkane) up to 33×10^7 s^{-1} (butyronitrile). in protic solvents from 13×10^7 s^{-1} (butanol) up to 60×10^7 s^{-1} (methanol). This behaviour is qualitatively similar and points to the involvement of a polar state responsible for these non-radiative losses (see above). A closer look at the Arrhenius activation energy E_A and pre-exponential factor log A in Table 2, however, reveals a striking difference. In alcohols, E_A decreases somewhat with increasing solvent polarity, as expected from the Bell–Evans–Polanyi correlation [47], and log A is more or less solvent independent, but in aprotic solvents, E_A increases with increasing solvent polarity, which would lead to decreased k_{nr}^T rates if no other factors were active. The experimentally observed increase in k_{nr}^T is brought about by the overcompensating effect of a strongly solvent-polarity-dependent pre-exponential factor A which increases by a factor of about 24 from non-polar alkane to polar butyronitrile. A similar behaviour has recently been observed in TICT formation kinetics where the observed rate differences for various dialkylaminobenzonitriles and esters are mainly due to the pre-exponential factor [52–54] whereas the activation energies are very similar for all the compounds [52,55]. With reference to Eyring's theory of the activated complex, this behaviour could be termed "entropically controlled" [56–60].

A possible explanation for this unusual behaviour can be found in the recent quantum-chemical extensions of the classical electron transfer theory [61,62] which allow ET reactions to proceed into vibrationally excited product states (broken parabolae in Fig. 7). In the case when ET is in the Marcus inverted region [62,63], the involvement of such "phonon-dressed" potential curves of the product ("nuclear tunnelling") leads to increased reaction rates mainly due to a lowering of the activation barrier for the vibrationally excited states of the product (Fig. 7(a), broken parabolae). This has recently been exemplified for the case of the solvent-polarity-dependent non-radiative decay in exciplexes [64]. If, however, ET occurs in the normal region (Fig. 7(b)), involvement of vibronically excited product states should lead to increased activation energies.

According to Arrhenius, the reaction rate, in our case the ET rate towards the TICT state, can be expressed by

$$k_{ET} = A \exp\left(-\frac{E_A}{k_B T}\right) \tag{4}$$

where E_A and A are the activation parameters and k_B is Boltzmann's constant. Within the ET theory the following equation can be used for expressing ET rates:

$$k_{ET} = \kappa\, FC \exp\left(-\frac{\Delta G^*}{k_B T}\right) \tag{5}$$

In (5), the pre-exponential term is composed of the electronic transmission factor κ and the Franck–Condon factor FC, which also contains the entropic contributions [61,65], the product of which can, by comparison of (4) and (5), be identified with the Arrhenius pre-exponential factor A. In the case of nuclear tunnelling, FC and ΔG^* correspond to effective values resulting from summation over the individual decay channels into the vibrationally excited product states with the individual activation energies ΔG^*_v depending on the vibrational quantum number v (Figs. 7(a) and 7(b)).

For the exciplex case where the reactant (exciplex) state R is excited and of CT character, and the product state P is the weakly polar ground state [64], increasing solvent polarity preferentially lowers the reactant state R and decreases the energy gap ΔG. We therefore expect smaller activation energies ΔG^*_v in Fig. 7(a) and the preferential involvement of less highly vibrationally excited product states. In the exciplex case these are believed to possess intrinsically larger FC factors [64]; hence the ET reaction rate increases with increasing solvent polarity owing to both a decreased activation energy and an increased A factor.

Our ET reaction is thought to take place at the excited-product-state A* hypersurface and therefore probably involves the normal Marcus region (Fig. 7(b)). As it leads from a non-polar reactant R to a polar excited product state P, increased solvent polarity will increase ΔG and therefore lower the activation energies ΔG^*_v for all product vibrational

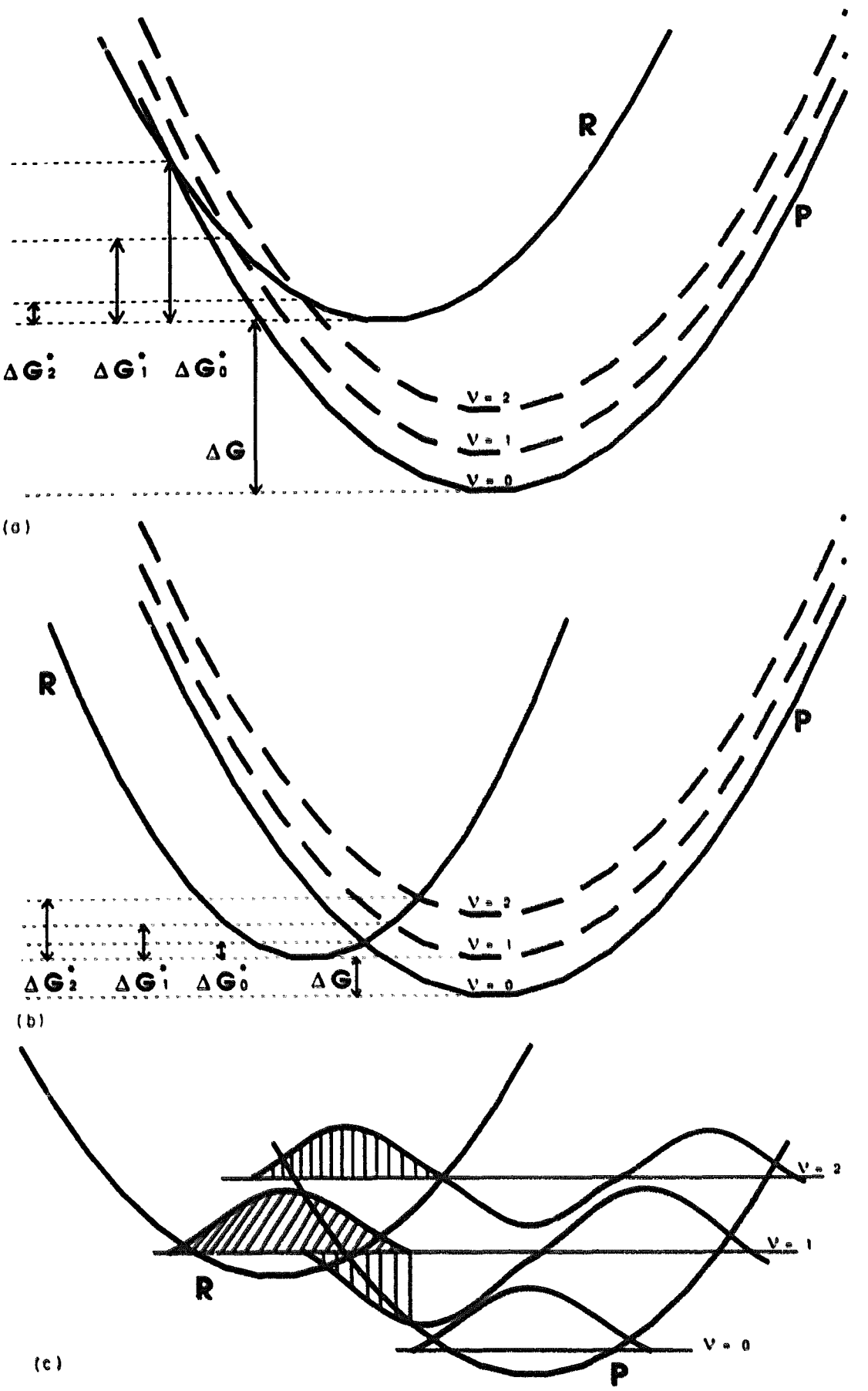

Fig. 7. Marcus parabola for reactant R and product P (a) in the case of the inverted Marcus region and (b) in the normal Marcus region: ——, zero vibrational levels of the respective states; – –, excited levels. In the inverted region (a), the activation free energy ΔG^*_v for each vibrational level decreases with increasing quantum number v, but increases in the case of the normal Marcus region (b). A decrease in the driving force ΔG has the same effect. (c) A schematic representation of the vibrational wavefunctions is shown, and the overlap region (shaded vertically) between the different product wavefunctions and the reactant wavefunction (shaded obliquely) is indicated, visualizing the increasing Franck–Condon factor for increasing quantum numbers v in this case.

levels. The involvement of nuclear tunnelling should be unimportant because of the increased ΔG^*_v for higher vibrational quantum numbers, unless the Franck–Condon term FC in Eq. (5) also increases for higher vibrational quantum numbers v. If this is the case, and if FC increases more strongly with increasing v than does the exponential term in Eq. (5), then nuclear tunnelling may be favourable also for ET processes in the normal Marcus region, and one would predict that ET will occur mainly into excited vibronic levels of P. Franck–Condon factors which increase with increasing v are quite normal for potentials with strongly displaced minima as schematically shown in Fig. 7(c). For the combination of ground and excited states, they are often directly visible from the relative intensities of vibronic band series in absorption

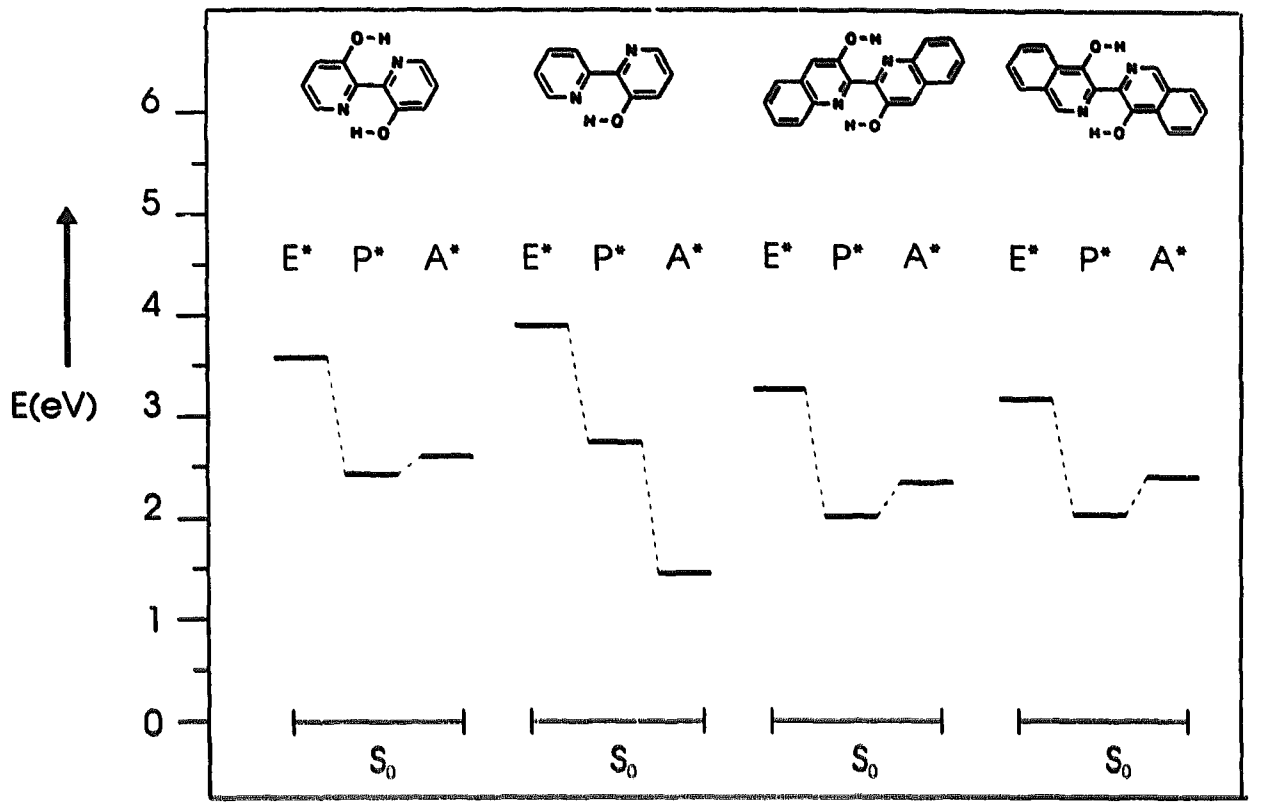

Fig. 8. Energetics of the three states relevant for the photophysics of the ESIPT dyes **1–3** possessing a flexible bond. E* and P* are calculated for planar structures; A* corresponds to the twisted structure of P*.

(or fluorescence) spectra, when the maximum occurs for a transition different from the series origin, e.g. in anthracene (medium frequency C–C stretching vibration) [66] or in 9,9′-bianthryl and related derivatives [67,68] (low frequency intramolecular librational motion).

To accommodate our observation of increased activation energies for increased solvent polarity within the quantum-chemical extension of classical ET theory, we therefore have to assume that, for increasing solvent polarity, the ET reaction occurs at vibrational levels of higher quantum number, favoured by larger Franck–Condon factors.

The question remains why we find evidence for nuclear tunnelling only in aprotic solvents. This difference is probably related to the different nature of the emissive species in aprotic and protic solvents. As discussed above, protic solvents lead to specifically solvated species (engaged in intermolecular solute–solvent H bonding) which show a slightly blue-shifted emission spectrum (Fig. 2) and exhibit an increased emission rate (from 8×10^7 s^{-1} in aprotic to 12×10^7 s^{-1} in protic solvents (Table 2)). The intermolecular H bonding weakens the intramolecular H bonding with the consequence that the rotational potential may become steeper in aprotic than in protic solvents, and this will impose an additional hindrance to any twisting motion in aprotic solvents. The TICT formation necessitates a twisting away from the planar conformation, and therefore a breaking of these intramolecular H bonds which are present in the aprotic solvents. ET, twisting motion and intramolecular H bonding are therefore more strongly coupled in aprotic solvents than in protic solvents, and it is conceivable that this coupling may necessitate a quantum-mechanical description.

5. Conclusions

Putting together both ESIPT and TICT photochemical reactions we propose that **2** and, to some extent, also **1** return to the ground state in aprotic polar solvents via a double-stage photochemical mechanism as indicated in Scheme 1. ESIPT kinetics are ultrafast such that fluorescence from the precursor enol species E* (and possible quenching by the respective TICT states of E* predicted to be higher in energy (Table 7)) is negligible. The ESIPT product species P* can react to a non-luminescent TICT state A*. Compounds **1** and **2** mainly differ in this photochemical channel, and the quantum-chemical calculations indicate that the reason for this difference is the energetics of A*. In protic solvents, this picture is complicated by the involvement of solute–solvent complexation. Furthermore, nuclear tunnelling probably connected with the rupture of H bonds is shown to be of importance in **1**.

The energetics of this consecutive three-state photochemical scheme are summarized in Fig. 8. This figure also contains the predictions for **3**, which has only very recently become available [69].

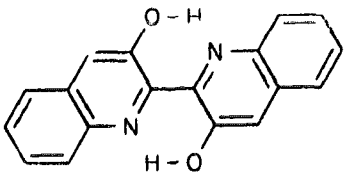

3

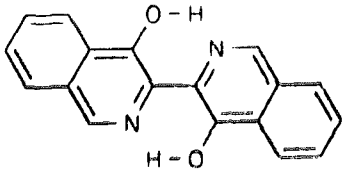

4

Because of a high-lying TICT state, **3** should show similarly good fluorescence quantum yields as **1**, but is absorption should be red shifted by about 0.2 eV to about 380 nm, and

its ESIPT emission is predicted to occur at around 560 nm. The calculations for **4** predict a very favourable quantum yield too, a high-lying TICT state and an absorption around 400 nm and its ESIPT emission around 620 nm. The latter examples show how mechanistic control can be used in predicting new and efficient ESIPT dyes of desired properties (longer-wavelength absorption to cover a better range of the solar spectrum and minimization of intramolecular non-radiative processes), e.g. for use in fluorescence solar concentrators or in proton transfer lasers.

Acknowledgements

We thank Professor A. Grabowska for samples of **1** and **2**. Discussions with A. Grabowska, Z.R. Grabowski, M. Van der Auweraer and K.H. Grellmann are highly appreciated. This work has been supported by the Technical University Berlin (Forschungsinitiativprojek FIP 6/10) and by the Bundesministerium für Forschung und Technologie (Project 05 314FAI5 and 05 414 FAB1). W.R. wishes to thank the Deutsche Forschungsgemeinschaft for a Heisenberg Fellowship during the time when most of this work was carried out.

References

[1] R. Reisfeld, *J. Non-Cryst. Solids, 121* (1990) 254.
[2] R. Reisfeld, M. Eyal, V. Chernyak and R. Zusman, *Sol. Energy Mater., 17* (1988) 439.
[3] W. Stahl and A. Zastrow, *Phys. Z., 16* (1985) 167.
[4] A. Goetzberger and W. Greubel, *Appl. Phys., 14* (1977) 123.
[5] W. Weber and H. Lampe, *Appl. Opt., 15* (1976) 10.
[6] R. Reisfeld and C.K. Jørgensen, *Struct. Bonding, 49* (1982) 1.
[7] G. Seybold and G. Wagenblast, *Dyes Pigments, 11* (1989) 303.
[8] R. Reisfeld, D. Brusilovsky, M. Eyal, E. Miron, Z. Burstein and J. Ivri, *Chem. Phys. Lett., 160* (1989) 43.
[9] R. Reisfeld, 'Luminescence and nonradiative processes in porous glasses', *International School of Atomic and Molecular Spectroscopy, 9th Course, Advances in Nonradiative Solids, Erice, 15–30 June 1989.*
[10] R. Reisfeld, D. Levy and D. Avenir, *J. Phys. Chem., 88* (1984) 5956.
[11] H. B[illegible]ska and A. Grabowska, *Pol. Pat. P 266542*, 1987.
[12] M. K[illegible], T.J. Aartsma, D. McMorrow and T. Chou, *J. Phys. Chem., 88* (1[illegible]34) 4596.
[13] P.F. Barbara and A.J.G. Strandjord, *J. Phys. Chem., 89* (1985) 2355.
[14] A.J.G. Strandjord, D.E. Smith and P.F. Barbara, *J. Phys. Chem., 89* (1985) 2362.
[15] A. Mordzinski, *Chem. Phys. Lett., 152* (1988) 151.
[16] B. Dick and P. Ernsting, *J. Phys. Chem., 91* (1987) 4261.
[17] J. Sepiol and R. Kolos, *Chem. Phys. Lett., 167* (1990) 445.
[18] J. Waluk, H. Bulska, A. Grabowska and A. Mordzinski, *Nouv. J. Chim., 10* (1986) 413.
[19] H. Langhals and S. Pust, *Chem. Ber., 118* (1985) 4674.
[20] H. Bulska, A. Grabowska and Z.R. Grabowski, *J. Lumin., 35* (1986) 189.
[21] H. Bulska, *Chem. Phys. Lett., 98* (1983) 398.
[22] J. Sepiol, H. Bulska and A. Grabowska, *Chem. Phys. Lett., 140* (1987) 607.
[23] H. Bulska, *J. Lumin., 39* (1988) 293.
[24] A. Costela, F. Amat, J. Catalán, A. Donhal, J.M. Figuera, J.M. Munoz and A.U. Aaina, *Opt. Commun., 64* (1987) 457.
[25] P. Chou and T.J. Aartsma, *J. Phys. Chem., 90* (1986) 721.
[26] Z.R. Grabowski, K. Rotkiewicz, A. Siemiarczuk, D.J. Cowley and W. Baumann, *Nouv. J. Chim., 3* (1979) 443.
[27] W. Rettig, *Angew. Chem., Int. Edn. Engl., 25* (1986) 971.
[28] E. Lippert, W. Rettig, V. Bonacic-Koutecký, F. Heisel and J.A. Miehé, *Adv. Chem. Phys., 68* (1987) 1.
[29] W. Rettig, in J. Liebman and A. Greenberg (eds.), *Modern Models of Bonding and Delocalization (Molecular Structure and Energetics*, Vol. 6), VCH, New York, 1988, p. 225.
[30] W. Rettig and W. Majenz, *Chem. Phys. Lett., 154* (1989) 335.
[31] R. Lapouyade, K. Czeschka, W. Majenz, W. Rettig, E. Gilabert and C. Rullière, *J. Phys. Chem., 96* (1992) 9643.
[32] J. Dobkowski, W. Rettig, B. Paeplow, K.H. Koch, K. Müllen and Z.R. Grabowski, *New J. Chem., 18* (1994) 525.
[33] W.H. Melhuish, *J. Phys. Chem., 65* (1961) 229; J.N. Demas and G.A. Crosby, *J. Phys. Chem., 75* (1971) 991; S.R. Meech and D. Phillips, *J. Photochem., 23* (1983) 193.
[34] M. Vogel and W. Rettig, *Ber. Bunsenges. Phys. Chem., 91* (1987) 1241.
[35] J. DelBene and H.H. Jaffé, *J. Chem. Phys., 48* (1968) 1807, 4050; *49* (1968) 1221; *50* (1969) 1126.
[36] *QCPE Program 333.*
[37] D.S. Viswanath and G. Natarajan, *Data Book on the Viscosity of Liquids*, Hemisphere, New York, 1989; *CRC Handbook of Chemistry and Physics*, CRC Press, Boca Raton, FL, 73rd edn., 1992–1993.
[38] P. Borowicz, A. Grabowska, R. Wortmann and W. Liptay, *J. Lumin., 52* (1992) 265.
[39] R. Wortmann, K. Elich, S. Lebus, W. Liptay, P. Borowicz and A. Grabowska, *J. Phys. Chem., 96* (1992) 9724.
[40] N.J. Turro, *Molecular Photochemistry*, Benjamin, New York, 1965, pp. 24, 48.
[41] M. Klessinger and J. Michl, *Lichtabsorption und Photochemie organischer Moleküle*, VCH, Weinheim, 1989, p. 205.
[42] W. Rettig, in J. Mattay (ed.), *Electron Transfer I*, in *Top. Curr. Chem., 160* (1994) 253.
[43] V. Bonacic-Koutecký and J. Michl, *J. Am. Chem. Soc., 107* (1985) 1765.
[44] V. Bonacic-Koutecký, J. Koutecký and J. Michl, *Angew. Chem., 99* (1987) 216; *Angew. Chem., Int. Edn. Engl., 26* (1987) 170.
[45] V. Bonacic-Koutecký, K. Schöffel and J. Michl, *J. Am. Chem. Soc., 111* (1989) 6140.
[46] J. Michl and V. Bonacic-Koutecký, *Electronic Aspects of Organic Photochemistry*, Wiley, New York, 1990.
[47] M.J.S. Dewar and R.C. Dougherty, *The PMO Theory of Organic Chemistry*, Plenum, New York, 1975, p. 212.
[48] W. Rettig, W. Majenz, R. Herter, J.F. Létard and R. Lapouyade, *Pure Appl. Chem., 65* (1993) 1699.
[49] W. Rettig, B. Strehmel and W. Majenz, *Chem. Phys., 173* (1993) 525.
[50] N. Nakashima, M. Murakawa and N. Mataga, *Bull. Chem. Soc. Jpn., 49* (1976) 854.
[51] W. Rettig and M. Zander, *Ber. Bunsenges. Phys. Chem., 87* (1983) 1143.
[52] W. Rettig and R. Gleiter, *J. Phys. Chem., 89* (1985) 4676.
[53] W. Rettig, *Bunsenges. Phys. Chem., 95* (1991) 259–263.
[54] W. Rettig, in N. Mataga, T. Okada and H. Masuhara (eds.), *Dynamics and Mechanisms of Photoinduced Electron Transfer and Related Phenomena*, Elsevier, Amsterdam, 1992, p. 57.
[55] W. Rettig, *J. Lumin., 26* (1981) 21–46.
[56] F.D. Lewis, R.W. Johnson and D.R. Kory, *J. Am. Chem. Soc., 96* (1974) 6100.
[57] K.N. Houk, N.G. Rondan and J. Mareda, *Tetrahedron, 41* (1985) 1555.
[58] J.R. Hurst and G.B. Schuster, *J. Am. Chem. Soc., 104* (1982) 6854.
[59] R.A. Moss, W. Lawrynowicz, N.J. Turro, I.R. Gould and Y. Cha, *J. Am. Chem. Soc., 108* (1986) 7028.

[60] V. Jagannadham and S. Steenken, *J. Am. Chem. Soc.*, *110* (1988) 2188.
[61] P. Siders and R.A. Marcus, *J. Am. Chem. Soc.*, *103* (1981) 741.
[62] J. Jortner and M. Bixon, *J. Chem. Phys.*, *88* (1988) 167.
[63] G.C. Walker, E. Akesson, A.E. Johnson, N.E. Levinger and P.F. Barbara, *J. Phys. Chem.*, *96* (1992) 3728.
[64] Ph. Van Haver, N. Helsen, S. Depaemelaere, M. Van der Auweraer and F.C. De Schryver, *J. Am. Chem. Soc.*, *113* (1991) 6849.
[65] N. Sutin, in V. Balzani (ed.), *Supramolecular Photochemistry*, Reidel, Dordrecht, 1987, p. 73.
[66] I.B. Berlman, *Handbook of Fluorescence Spectra of Aromatic Molecules*, Academic Press, New York, 1971.
[67] A. Subaric-Leitis, Ch. Monte, A. Roggan, W. Rettig, P. Zimmermann and J. Heinze, *J. Chem. Phys.*, *93* (1990) 4543.
[68] C. Monte, A. Roggan, A. Subaric-Leitis, W. Rettig and P. Zimmermann, *J. Chem. Phys.*, *98* (1993) 2580.
[69] H. Langhals, *J. Synth. Org. Chem.*, *4* (1990) 259.